Front. Phys. 13(2), 137102 (2018)
https://doi.org/10.1007/s11467-017-0723-5

RESEARCH ARTICLE

Elastic, dynamical, and electronic properties of LiHg and Li_3Hg: First-principles study

Yan Wang (王研), **Chun-Mei Hao** (郝春梅), **Hong-Mei Huang** (黄红梅)†, **Yan-Ling Li** (李延龄)

School of Physics and Electronic Engineering, Jiangsu Normal University, Xuzhou 221116, China
Corresponding author. E-mail: †hmhuang@jsnu.edu.cn
Received April 26, 2017; accepted August 27, 2017

The elastic, dynamical, and electronic properties of cubic LiHg and Li_3Hg were investigated based on first-principles methods. The elastic constants and phonon spectral calculations confirmed the mechanical and dynamical stability of the materials at ambient conditions. The obtained elastic moduli of LiHg are slightly larger than those of Li_3Hg. Both LiHg and Li_3Hg are ductile materials with strong shear anisotropy as metals with mixed ionic, covalent, and metallic interactions. The calculated Debye temperatures are 223.5 K and 230.6 K for LiHg and Li_3Hg, respectively. The calculated phonon frequency of the T_{2g} mode in Li_3Hg is 326.8 cm^{-1}. The p states from the Hg and Li atoms dominate the electronic structure near the Fermi level. These findings may inspire further experimental and theoretical study on the potential technical and engineering applications of similar alkali metal-based intermetallic compounds.

Keywords Li-Hg alloys elastic property phonon spectrum electronic structure

PACS numbers 71.20.Lp, 62.20.-x, 63.20.D-

1 Introduction

Intermetallic compounds have attracted intense interest on their bound properties, low metallic conductivities, and lattice defects [1, 2]. The characteristics of crystal structure ordering and the coexistence of metallic and covalent bonds endow intermetallic compounds with many outstanding properties.

In recent decades, alkali metal-based intermetallic compounds, such as I–II and I–III metal compounds, have been of intense interest to researchers for their potential technological applications [3]. Most of these compounds crystallize in the $B32$ NaTl-type structure at ambient conditions, abiding by the Zintl–Klemn concept. Some exceptions, such as LiTl and LiHg, crystallize in the $B2$ CsCl-type structure because of the atomic size effect, which defies the Zintl–Klemn concept [4].

LiHg has been widely investigated by molecular beam scattering experiments [5, 6], *ab initio* calculations [7], and laser-assisted spectroscopy [8–10] because of its potential application as a laser medium [11]. For the Li–Hg system, LiHg and Li_3Hg compounds were reported and assigned as cubic in structure in the early 20^{th} century [12]. However, few theoretical or experimental studies on their physical properties exist. Christensen explored the structural phase stability of LiHg based on first-principles methods [3], finding that LiHg was much more stable in the $B2$ structure than in the $B32$ structure, in agreement with experimental observations. Recently, the polarities of Li_3Hg, LiHg, and $LiHg_3$ were investigated via nuclear magnetic resonance (NMR) methods combined with *ab initio* band structure calculations, demonstrating that charge transfer was generally more pronounced in more Hg-rich amalgams, because larger Hg sublattices can more efficiently delocalize negative charges [13]. The lack of reports on the mechanical and dynamical properties of LiHg and Li_3Hg compounds is unexpected. The elastic behavior and dynamical properties of such materials must be determined to fully understand their physical properties and potential applications.

Here, the elastic, dynamical, and electronic properties of LiHg and Li_3Hg were studied using first-principles calculations within the framework of the density functional theory (DFT). The mechanical and dynamical stability of LiHg and Li_3Hg were determined by calculating their elastic constants and phonon spectra. The elastic anisotropy and dynamical behaviors were explored and their electronic structures were discussed.

2 Calculation methods

The electronic properties were calculated using DFT within the generalized-gradient approximation (GGA) [14] as implemented in the Vienna *ab initio* simulation package (VASP) [15], employing the projected augmented-wave (PAW) pseudopotential included in the released pseudopotential library [16, 17]. The electronic wave function was expanded using the plane-wave basis with the cut-off energy of 650 eV. During the geometry optimization, the convergence threshold was 1.0×10^{-6} eV/atom for the maximum energy change and 0.001 eV/Å for the maximum force. The convergence threshold in the self-consistent field calculation was also 1.0×10^{-6} eV/atom. The electronic Brillouin zone (BZ) integration was based on a $16 \times 16 \times 16$ array of Monkhorst–Pack k-point meshes for LiHg and $12 \times 12 \times 12$ for Li_3Hg. The elastic constants were calculated by the finite strain technique within the framework of the linear response theory. The phonon dispersion was obtained in terms of the Quantum-Espresso package [18] using the PAW pseudopotential [16, 17] with the cutoff energies of 50 Ry and 500 Ry for the wave functions and the charge density, respectively. The dynamic matrix was computed based on a $4 \times 4 \times 4$ mesh of phonon wave vectors.

3 Results and discussion

3.1 Structural property

LiHg crystallizes in the CsCl-type structure (space group Pm-$3m$) in which each lithium atom is surrounded by eight mercury atoms [see Fig. 1(a)], while Li_3Hg possesses the Fe_3Al-type structure (space group Fm-$3m$) [see Fig. 1(b)]. For Li_3Hg, the lithium atoms hold two different crystallographic positions, referred to as Li1 4b and Li2 8c. The optimized equilibrium lattice parameters are 6.5257 Å for Li_3Hg and 3.3413 Å for LiHg, in good agreement with available experimental values [12]. As a result, the density is increased by 74.6% from 5.292 g/cm^3 for the Li-rich Li_3Hg to 9.238 g/cm^3 for LiHg.

3.2 Elastic properties

The elastic constants determine the stiffness of a crystal against externally applied strains. The calculated elastic constants are given in Table 1. For a stable cubic structure, the three independent elastic constants (C_{11}, C_{12}, and C_{44}) should match the well-known Born criteria for stability [19] of $C_{44} > 0$, $C_{11} > |C_{12}|$, and $C_{11}+2C_{12} > 0$. Obviously, the calculated elastic constants C_{ij} for LiHg and Li_3Hg satisfy the mechanical stability criteria, indicating the mechanical stability of the compounds. Using the calculated elastic constants, it is easy to calculate the bulk modulus B and shear modulus G [20–24]. The obtained bulk moduli are 30.0 GPa for LiHg and 25.7 GPa for Li_3Hg (see Table 2). The Young's modulus E and Poisson's ratio ν are then calculated, considering their importance in technological and engineering applications (see Table 2). In order to estimate the brittle and ductile behaviors of materials, Pugh [25] suggested the ratio of the bulk to shear modulus (B/G) of polycrystalline

Table 1 Independent elastic constants C_{ij} (GPa), space groups, and Zener anisotropy indices A of LiHg and Li_3Hg.

Compound	Space group	C_{11}	C_{12}	C_{44}	A
LiHg	Pm-$3m$	54.5	17.8	26.4	1.44
Li_3Hg	Fm-$3m$	32.6	22.3	21.8	4.22

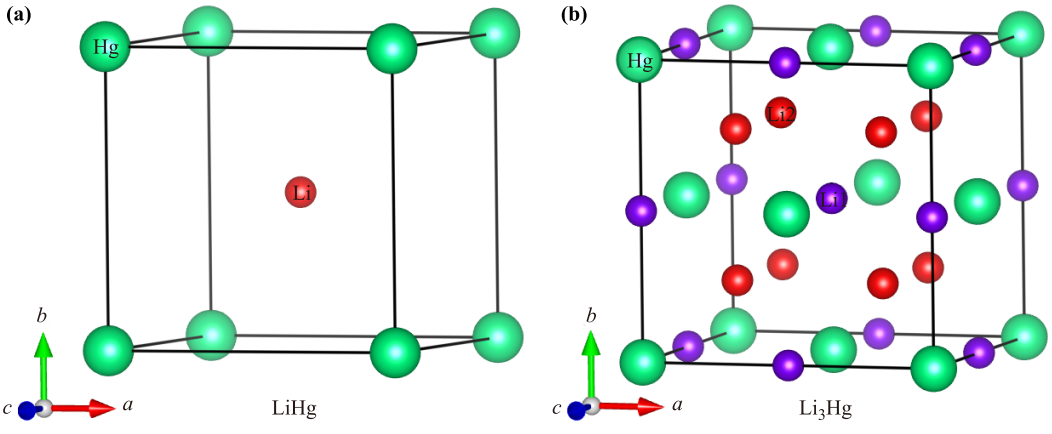

Fig. 1 Crystal structures of **(a)** LiHg and **(b)** Li_3Hg. The red and orange balls represent the lithium atoms, and the green balls, the mercury atoms.

Table 2 Bulk moduli B (GPa), shear moduli G (GPa), Young's moduli E (GPa), Poisson's ratios ν, Debye temperatures Θ_D (K), and B/G ratios of LiHg and Li_3Hg.

Compound	B	G	E	Θ_D	ν	B/G
LiHg	30.0	30.5	44.2	223.5	0.12	0.98
Li_3Hg	25.7	17.4	24.1	230.6	0.22	1.44

phases, considering B as the resistance to fracture and G as the resistance to plastic deformation. Therefore, high and low B/G values are associated with ductility and brittleness, respectively. The critical ratio separating ductile and brittle materials is approximately 1.75 [26]. From Table 2, the calculated values of B/G for both LiHg and Li_3Hg are below 1.75, suggesting that both LiHg and Li_3Hg are brittle, particularly LiHg.

The elastic anisotropy of the material must be determined to permit application in engineering science [20, 21, 26, 27]. C_{44} represents the resistance to deformation by shearing stresses applied across the (100) plane in the [010] direction; $(C_{11} - C_{12})/2$ represents the resistance to shear deformation by shearing stress applied across the (110) plane in the [1–10] direction. The Zener anisotropy index [28], $A = 2C_{44}/(C_{11} - C_{12})$, provides insight on the elastic anisotropy of the present two compounds. For isotropic systems, A has the value of 1, while values greater or smaller than unity indicate the extent of elastic anisotropy. The calculated values of A for LiHg and Li_3Hg (see Table 1) indicate that Li_3Hg has stronger shear anisotropy than LiHg.

The Debye temperature correlates with many physical properties of solids, such as the specific heat, elastic stiffness constants, and melting temperature [20, 21, 27]. Therefore, we estimated the Debye temperature by using the bulk modulus, shear modulus, and density [26, 27]. The calculated Debye temperatures ($\Theta_D s$) are 223.5 K for LiHg and 230.6 K for Li_3Hg.

3.3 Dynamical properties

Phonon calculations indicate that LiHg and Li_3Hg are dynamically stable at zero pressure. The phonon dispersions and partial phonon densities of states (PPDOS) of LiHg and Li_3Hg are shown in Figs. 2(a) and (b), respectively. The maximum optical branch frequency is 291.5 cm^{-1} for LiHg, which is lower than the 375.8 cm^{-1} frequency of Li_3Hg because of obvious structural differences. Unlike in LiHg, two inequivalent lithium atoms exist in Li_3Hg, as mentioned above. The bond length between lithium and mercury atoms in Li_3Hg is 2.826 Å, shorter than the 2.894 Å bond length of LiHg, in-

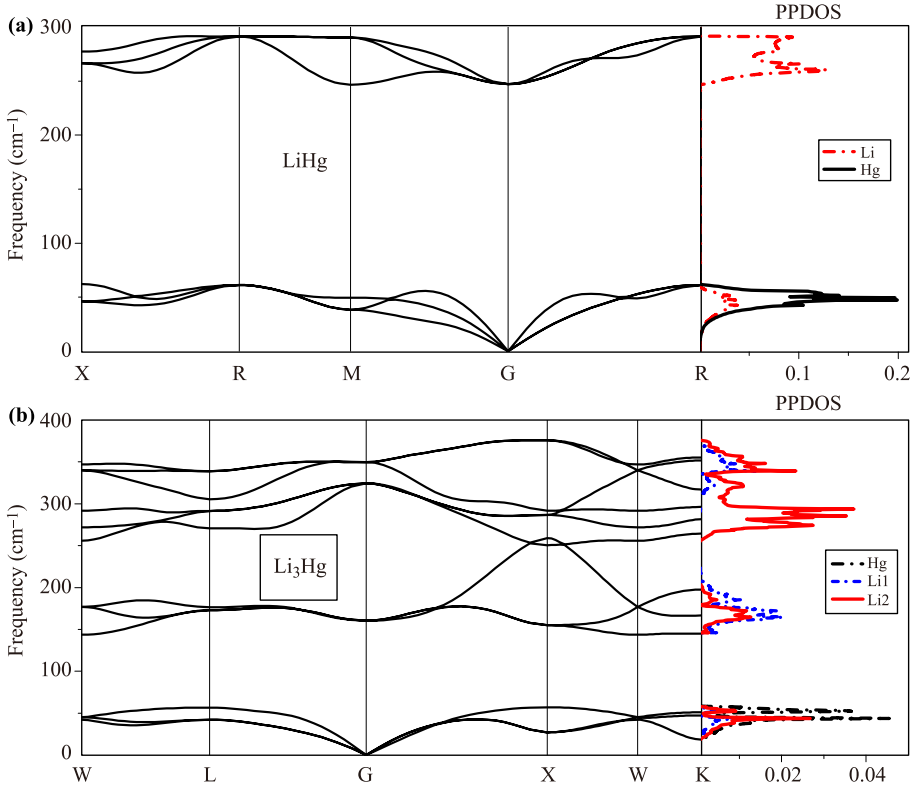

Fig. 2 Phonon dispersions and partial phonon density of states (PPDOS) for **(a)** LiHg and **(b)** Li_3Hg.

dicating stronger interatomic interactions in Li_3Hg. In addition, strong covalent bonding exists between Li1 and Li2 atoms in Li_3Hg, as is discussed later. These factors promote the higher maximum optical branch frequency in Li_3Hg relative to that in LiHg.

From the PPDOS, the acoustic branches mainly originate from the vibrations of mercury atoms, but the optical branches only arise from the vibrations of lithium atoms, attributed to the small mass ratio between the lithium and mercury atoms. The observed frequency gap (86.6 cm^{-1}) in Li_3Hg is far lower than that (184.4 cm^{-1}) in LiHg, which is attributed to the strong phonon hybridization from the Li1 and Li2 atoms in the optical branches of Li_3Hg [see Fig. 2(b)]. Such frequency gaps are regularly observed in covalent systems [21, 29]. Symmetry analysis shows that no Raman-active mode occurs in LiHg. For Li_3Hg, a triplet Raman-active mode exists with T_{2g} symmetry. The calculated phonon frequency of the T_{2g} mode is 326.8 cm^{-1}.

3.4 Electronic properties

The energy bands of LiHg and Li_3Hg along the high-symmetry directions in the BZ are plotted in Fig. 3. Obviously, these two compounds exhibit metallic characters because some bands cross the Fermi levels. The projected densities of states (PDOS) near the Fermi level are given in Fig. 4, where the vertical lines indicate the Fermi levels E_F. Conducting behavior dominates the Hg-p orbital and Li-p orbital, whereas Li-s, Hg-s, and Hg-d electrons make minor contributions to the DOS near E_F. Therefore, the p states from the mercury and lithium atoms are mainly responsible for the electronic properties of the LiHg and Li_3Hg compounds. Although both compounds are metals, the electronic structures differ significantly, indicating changes in the chemical bonding situations between the two. The band gap from −4.567 eV to −2.375 eV located in the band structure of Li_3Hg is closed in LiHg through the broadening of Hg-s and Hg-d states.

The electron localization functions (ELFs) of LiHg and Li_3Hg (see Fig. 5) were calculated for bonding analysis because ELF provides a useful measure. The results show that electrons are transferred from lithium to mercury, which naturally arises from the obvious electronegativity difference in the constituent elements. To further evaluate the charge transfer, Mulliken atomic population analysis is performed by means of CASTEP code [30]. The total charge transfer from lithium to mercury in LiHg is 1.57|e|. For Li_3Hg, the charge transfer calculated from Li1 to Hg and that from Li2 to Hg are 0.51|e| and 0.97|e|, respectively. The obvious charge transfer from lithium to mercury atoms implies that the chemical bonding between Li and Hg has some ionic characteristics. The lithium-rich Li_3Hg system presents stronger ionic bonding compared to the LiHg system,

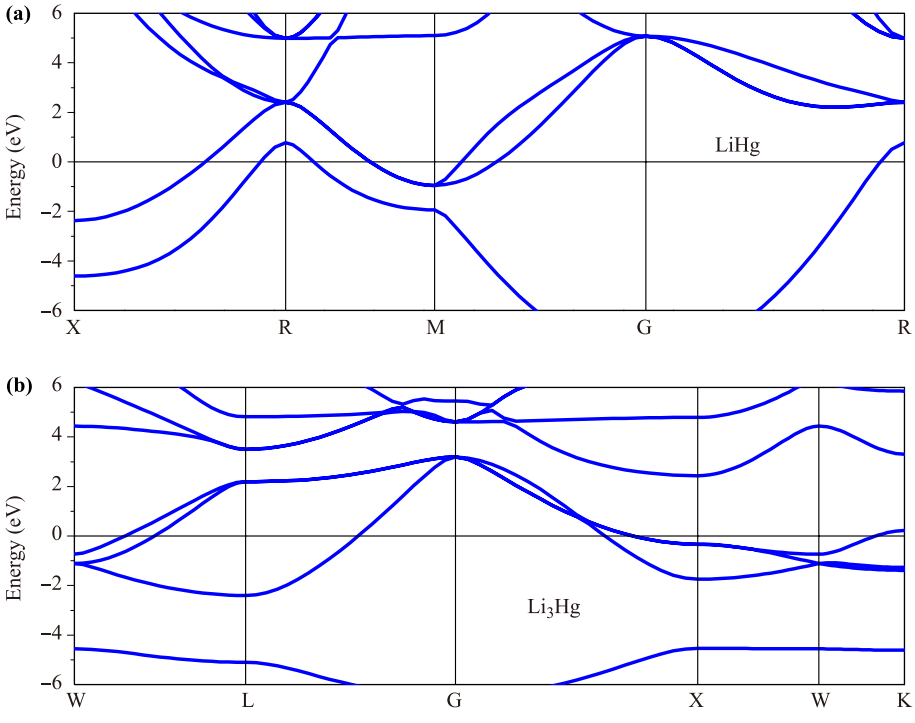

Fig. 3 The energy band structures of LiHg and Li_3Hg.

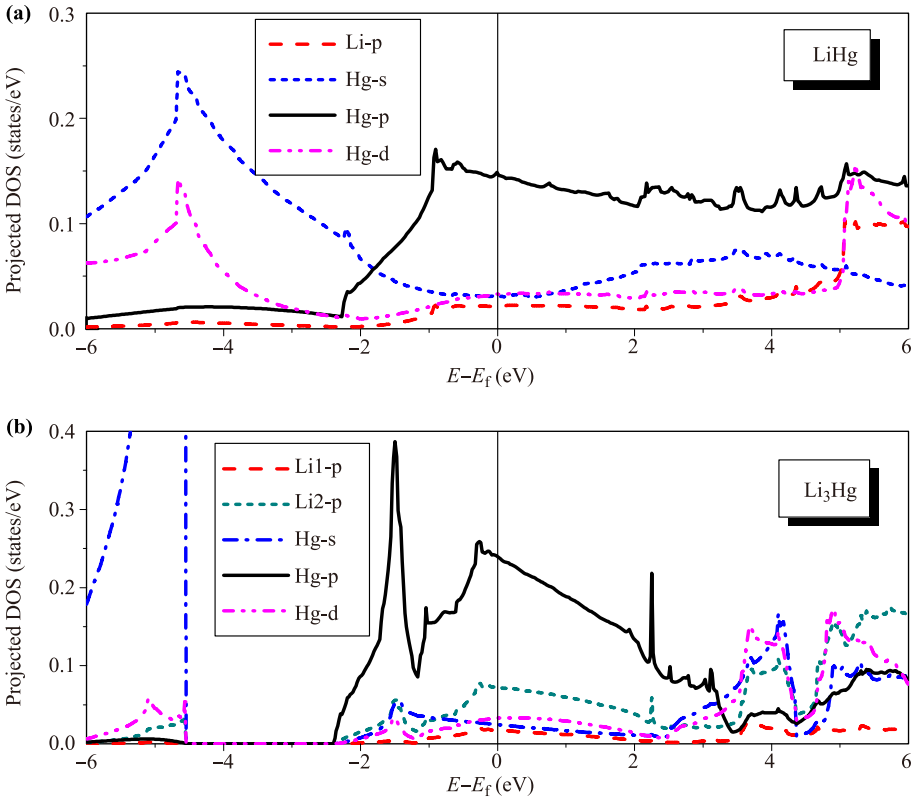

Fig. 4 Projected densities of states (PDOS) for LiHg and Li_3Hg.

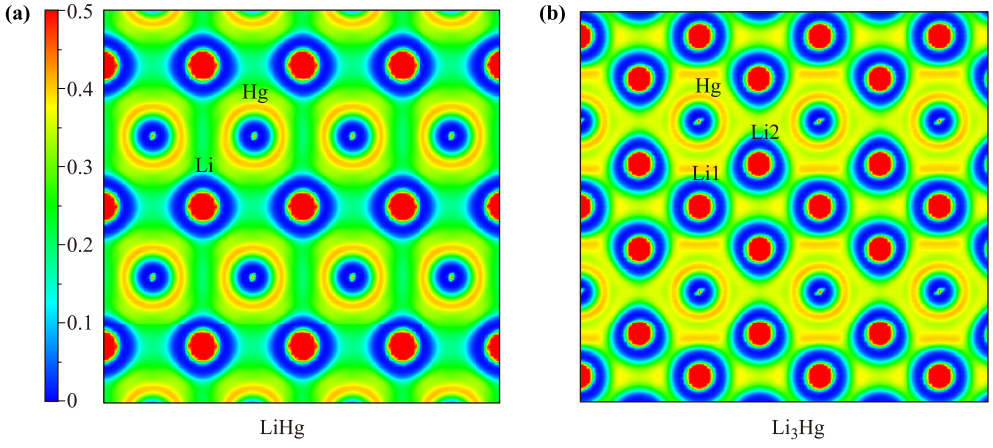

Fig. 5 Electron localization function (ELF) for **(a)** LiHg with an isosurface value of 0.42 and **(b)** for Li_3Hg 0.38, showing charge transfer from lithium to mercury atoms and covalent interactions.

which causes the slightly lower bulk modulus of Li_3Hg compared to LiHg. From Fig. 5, charge accumulates between the lithium atoms, indicating that directional bonding exists between the Li atoms (i.e., the Li1–Li2 bonding exhibits covalent characteristics). Thus, we can conclude that the bonds in LiHg and Li_3Hg should mix metallic, covalent, and ionic attributes. This phenomenon has also been observed in other intermetallic compounds, such as the K–Hg system [13]. The interplay of the three bonding types creates special electronic structures and thus promotes interesting physical properties, such as low metallic conductivity and high specific resistance. The covalent interactions between Li1 and Li2 in Li_3Hg cause stronger phonon coupling between lithium atoms, thus both decreasing the frequency gap mentioned above and increasing the optical vibration

modes [see Fig. 2(b)].

4 Conclusion

In summary, the mechanical, dynamical, and electronic properties of LiHg and Li_3Hg were explored by first-principles total energy calculation methods. The calculated elastic constants and phonon spectra indicated their mechanical and dynamical stability. The mechanical analysis showed that both LiHg and Li_3Hg are ductile materials with low elastic moduli and strong shear anisotropy. The electronic structure calculation revealed that both LiHg and Li_3Hg were metallic showing mixed chemical bonding, with coexistent ionic, covalent, and metallic bond characteristics.

Acknowledgements This study was supported by the National Natural Science Foundation of China under Grant Nos. 11347007 and 11674131, the Qing Lan Project, the Colleges and Universities in Jiangsu Province Natural Science Research Project under Grant No 14KJB460013, and the Priority Academic Program Development of Jiangsu Higher Education Institutions. Y. L. Li thanks the support from the Chinese Scholarship Council. C. M. Hao thanks the support from the Postgraduate Research & Practice Innovation Program of Jiangsu Province under Grant No. KYCX17_1652.

References

1. S. Kauzlarich, Chemistry, Structure and Bonding of Zintl Phases and Ions, New York: VCH Publishers, 1996
2. K. Kishio and J. O. Brittain, Defect structure of β-LiAl, *J. Phys. Chem. Solids* 40(12), 933 (1979)
3. N. E. Christensen, Structural phase stability of $B2$ and $B32$ intermetallic compounds, *Phys. Rev. B* 32(1), 207 (1985)
4. F. Wang and G. J. Miller, Revisiting the Zintl–Klemm concept: Alkali metal trielides, *Inorg. Chem.* 50(16), 7625 (2011)
5. R. E. Olson, Determination of the Li–Hg intermolecular potential from molecular-beam scattering measurements, *J. Chem. Phys.* 49(10), 4499 (1968)
6. U. Buck, H. O. Hoppe, F. Huisken, and H. Pauly, Intermolecular potentials by the inversion of molecular beam scattering data (IV): Differential cross sections and potential for LiHg, *J. Chem. Phys.* 60(12), 4925 (1974)
7. M. M. Gleichmann and B. A. Hess, Relativistic all-electron *ab initio* calculations of ground and excited states of LiHg including spin–orbit effects, *J. Chem. Phys.* 101(11), 9691 (1994)
8. D. Gruber and X. Li, Vibrational constants and long-range potentials of the LiHg (X_{12}) ground state, *Chem. Phys. Lett.* 240(1–3), 42 (1995)
9. D. Gruber, L. Windholz, X. Li, M. Gleichmann, and B. He, Theoretical and experimental studies of th LiHg-blue green bands, *AIP Conf. Proc.* 328, 406 (1995)
10. D. Gruber, X. Li, L. Windholz, M. Gleichmann, B. A. Hess, I. Vezmar, and G. Pichler, The LiHg($2^2\Pi 3/2$ – $X^2\Sigma^+_{1/2}$) system, *J. Phys. Chem.* 100(24), 10062 (1996)
11. D. Gruber, M. Musso, L. Windholz, M. Gleichmann, B. A. Hess, F. Fuso, and M. Allegrini, Study of the LiHg excimer: Blue–green bands, *J. Chem. Phys.* 101(2), 929 (1994)
12. L. F. Kozin and S. C. Hansen, Mercury Handbook: Chemistry, Applications and Environmental Impact, United Kingdom: Royal Society of Chemistry publishing, 2013
13. F. Tambornino and C. Hoch, Bad metal behaviour in the new Hg-rich amalgam KHg_6 with polar metallic bonding, *J. Alloys Compd.* 618, 299 (2015)
14. J. P. Perdew, K. Burke, and M. Ernzerhof, Generalized gradient approximation made simple, *Phys. Rev. Lett.* 77(18), 3865 (1996)
15. G. Kresse and J. Furthmüller, Efficiency of ab-initio total energy calculations for metals and semiconductors using a plane-wave basis set, *Comput. Mater. Sci.* 6(1), 15 (1996)
16. P. E. Blöchl, Projector augmented-wave method, *Phys. Rev. B* 50(24), 17953 (1994)
17. G. Kresse and D. Joubert, From ultrasoft pseudopotentials to the projector augmented-wave method, *Phys. Rev. B* 59(3), 1758 (1999)
18. P. Giannozzi, et al., QUANTUM ESPRESSO: A modular and open-source software project for quantum simulations of materials, *J. Phys.: Condens. Matter* 21, 395502 (2009)
19. M. Born and K. Huang, Dynamical Theory of Crystal Lattices, Oxford: Clarendon Press, 1956
20. Y. L. Li and Z. Zeng, Potential ultra-incompressible material ReN: First-principles prediction, *Solid State Commun.* 149(39–40), 1591 (2009)
21. Y. Li, Z. Zeng, and H. Lin, Structural, elastic, electronic and dynamical properties of OsB and ReB: Density functional calculations, *Chem. Phys. Lett.* 492(4–6), 246 (2010)
22. Y. L. Li, W. Luo, X. J. Chen, Z. Zeng, H. Q. Lin, and R. Ahuja, Formation of Nanofoam carbon and re-emergence of Superconductivity in compressed CaC_6, *Sci. Rep.* 3(1), 3331 (2013)
23. Y. L. Li, W. Luo, Z. Zeng, H. Q. Lin, H. K. Mao, and R. Ahuja, Pressure-induced superconductivity in CaC_2, *Proc. Natl. Acad. Sci. USA* 110(23), 9289 (2013)
24. R. Hill, The elastic behaviour of a crystalline aggregate, *Proc. Phys. Soc. Lond.* 65(5), 349 (1952)
25. S. F. Pugh, XCII. Relations between the elastic moduli and the plastic properties of polycrystalline pure metals, *Philos. Mag.* 45(367), 823 (1954)

26. P. Ravindran, L. Fast, P. A. Korzhavyi, B. Johansson, J. Wills, and O. Eriksson, Density functional theory for calculation of elastic properties of orthorhombic crystals: Application to $TiSi_2$, *J. Appl. Phys.* 84(9), 4891 (1998)

27. Y. L. Li and Z. Zeng, Structural, elastic, and electronic properties of ReO_2, *Chin. Phys. Lett.* 25(11), 4086 (2008)

28. C. Zener, Elasticity and Anelasticity of Metals, Chicago: Chicago University Press, 1948

29. Y. L. Li, S. N. Wang, A. R. Oganov, H. Gou, J. S. Simth, and T. A. Strobel, Investigation of exotic stable calcium carbides using theory and experiment, *Nat. Commun.* 6, 6974 (2015)

30. S. J. Clark, M. D. Segall, C. J. Pickard, P. J. Hasnip, M. J. Probert, K. Refson, and M. C. Payne, First principles methods using CASTEP, *Z. Kristallogr.* 220(5–6), 567 (2005)